

# An introduction to the parton and hadron cascade model PACIAE 3.0

An-Ke Lei,<sup>1</sup> Yu-Liang Yan,<sup>2,\*</sup> Dai-Mei Zhou,<sup>1,†</sup> Zhi-Lei She,<sup>3</sup> Liang Zheng,<sup>4</sup>  
Gao-Chan Yong,<sup>5,6</sup> Xiao-Mei Li,<sup>2</sup> Gang Chen,<sup>4</sup> Xu Cai,<sup>1</sup> and Ben-Hao Sa<sup>1,2,‡</sup>

<sup>1</sup>*Key Laboratory of Quark and Lepton Physics (MOE) and Institute of Particle Physics,  
Central China Normal University, Wuhan 430079, China*

<sup>2</sup>*China Institute of Atomic Energy, P. O. Box 275 (10), Beijing 102413, China*

<sup>3</sup>*School of Mathematical and Physical Sciences, Wuhan Textile University, Wuhan 430200, China*

<sup>4</sup>*School of Mathematics and Physics, China University of Geosciences (Wuhan), Wuhan 430074, China*

<sup>5</sup>*School of Nuclear Science and Technology, University of Chinese Academy of Sciences, Beijing 100049, China*

<sup>6</sup>*Institute of Modern Physics, Chinese Academy of Sciences, Lanzhou 730000, China*

(Dated: September 12, 2023)

We introduce a parton and hadron cascade model PACIAE 3.0 based on PYTHIA 6.428 and the PACIAE 2.2 program series. The simulation framework of C-, B-, and A-loops are designed for the high energy ( $\sqrt{s_{NN}} \geq 3$  GeV) and low energy ( $\sqrt{s_{NN}} < 3$  GeV) nuclear collisions, respectively, in PACIAE 3.0. In the C-loop simulation, the parton-parton inelastic scattering processes are added in the partonic rescattering process. The single string structure and multiple string interaction mechanism have been introduced investigating the strangeness enhancement in C- and B-loop. An improved mapping relation between the centrality percentage definition and the impact parameter definition is proposed responding the observation of  $b_{max} \approx 20$  fm from ALICE, ATLAS, and CMS collaborations. We have extensively modified the phenomenological coalescence hadronization model. The PACIAE 3.0 model simulated results of particle yield, transverse momentum distribution, and rapidity distribution well reproduce, respectively, the experimental data measured at FOPI, E895, RHIC, and LHC energies.

## I. INTRODUCTION

The phenomenological model-based Monte Carlo simulation is a powerful tool to investigate the relativistic nuclear collisions and Quark Gluon Plasma (QGP) phase transition observed there. To the end, various models have been developed, such as PYTHIA [1, 2], HERWIG [3], SHERPA [4], PCM [5], HIJING [6], QGSM [7], UrQMD [8], AMPT [9], PACIAE [10], THERMINATOR [11], PHSD [12], EPOS-LHC [13], SMASH [14], JETSCAPE [15] and Angantyr [16] in the high energy sector. At low energy the BUU-like models (such as BLOB, BUU-VM, DJBUU, GiBUU, IBL, IBUU, LBUU, pBUU, PHSD, RBUU, RVUU, SMASH, SMF,  $\chi$ BUU) and the QMD-like models (e.g., AMD, AMD+JAM, BQMD, CoMD, ImQMD, IQMD-BNU, IQMD-SINAP, JAM, JQMD, LQMD, TuQMD/dcQMD, UrQMD) are developed, cf. [17–19] and references therein.

PACIAE 3.0 is a parton and hadron cascade phenomenological model based on PYTHIA [1] and PACIAE 2.2 series [10, 20–23]. PACIAE model is developed from the LUCIAE [24–26] and JPCIAE [27] models. LUCIAE model was based on the FRITIOF [28] with the extension of implementing both the Firecracker model (collective multi-gluon emission in the interacting string color field) and the hadronic rescattering. JPCIAE model was based on the JETSET and PYTHIA [29] being able to simulate the relativistic hadron-hadron and heavy-ion collisions.

Soon after, the JETSET had been blended in PYTHIA, the JPCIAE was renamed as PACIAE 1.0 correspondingly. As quoted in [30], not only the LUCIAE model but also the JPCIAE (PACIAE 1.0) and even PACIAE 3.0 model are all based on LUND String Fragmentation (LSF) regime.

In PACIAE 3.0 the C-, B- and A-simulation loops are designed for the high energy ( $\sqrt{s_{NN}} \geq 3$  GeV) and low energy ( $\sqrt{s_{NN}} < 3$  GeV) nuclear collisions, respectively. In all the simulation loops the basic building block is a hadron-hadron ( $hh$ ) collision. The high energy  $hh$  collision is a large momentum transfer and small spatial scale process. It should be described first in the partonic degree of freedom and then hadronized into the hadronic degree of freedom of the final hadronic state by interfacing to PYTHIA [1]. The low energy  $hh$  collision can be dealt with the elastic and inelastic two-body scattering kinematics in hadronic degree of freedom only.

A couple of improvements in physics are introduced in PACIAE 3.0. They are listed as follows:

- (1) The  $hh$  total cross section is assumed to be proportional to the nucleon-nucleon ( $NN$ ) total cross section with coefficient equal to the ratio of effective valence quark number in  $hh$  collision system to that in  $NN$  collision system [30, 31]. And the experimentally measured  $NN$  total cross section [32] is adopted.
- (2) Three inelastic parton-parton scattering processes are added at partonic rescattering stage in the C-loop simulation.
- (3) Two strangeness enhancement mechanisms of single string structure and multiple string interaction

\* yanyl@ciae.ac.cn

† zhoudm@mail.ccnu.edu.cn

‡ sabh@ciae.ac.cn

are implemented in the B- and C-loop simulations.

- (4) An improved mapping relation between percentage centrality definition and impact parameter centrality definition responding the ALICE, ATLAS, and CMS observation of  $b_{max} \approx 20$  fm [10, 23] is proposed.
- (5) The phenomenological coalescence hadronization model is extensively modified in the C-loop simulation.

The PACIAE 3.0 program is now available on the open source platforms GitHub and Gitee <sup>1</sup>.

## II. CUMULATIVE SUPERPOSITION OF HADRON-HADRON COLLISIONS

To begin with a heavy-ion collision simulation one first distributes the nucleons in its own nucleus sphere by the Woods-Saxon distribution (for radius  $r$ ) and the uniform distribution in  $4\pi$  solid angle (for direction), as shown in Fig. 1. Here the time origin is set at the moment of two centers of the projectile and target spheres have the same coordinate of  $z = 0$  [10, 21, 33].

Takeing the Au+Au collision at  $\sqrt{s_{NN}} = 7.7$  GeV with the impact parameter  $b = 7$  fm as an example, the initial momentum of each nucleon in the projectile nucleus (Proj.) is  $p_x = p_y = 0$  and  $p_z = p_{beam}$ , and is  $p_x = p_y = 0$  and  $p_z = -p_{beam}$  in the target nucleus (Targ.). The Lorentz contraction is then performed. Figs. 1 and 2 show the initial spatial distribution of nucleons before and after Lorentz contraction, respectively. Meanwhile, the initial particle list, composed of four spatial and four momentum vectors of all nucleons in the Au+Au collision system, is constructed.

We assume the nucleon trajectory in the velocity field of nuclear collision system is a straight line. A nucleon  $i$  from projectile nucleus and  $j$  from target nucleus may collide if their relative transverse distance,  $D$ , satisfies

$$D \leq \sqrt{\sigma_{NN}^{tot}/\pi}, \quad (1)$$

where  $\sigma_{NN}^{tot}$  refers to the  $NN$  total cross section. The collision time  $t_{ij}$  is then calculated [10].

Two circulation loops are set: one for  $i$  cycling over all the projectile nucleons, another one for  $j$  cycling over all the target nucleons. With the calculated collision time  $t_{ij}$  of all  $i$ - $j$  pairs the initial  $NN$  collision time list is constructed for a heavy-ion collision system.

A  $NN$  collision with the least collision time is selected from the list. If it is properly executed (see next section) its final hadronic state is available and the generated hadrons are counted as its contribution to the final

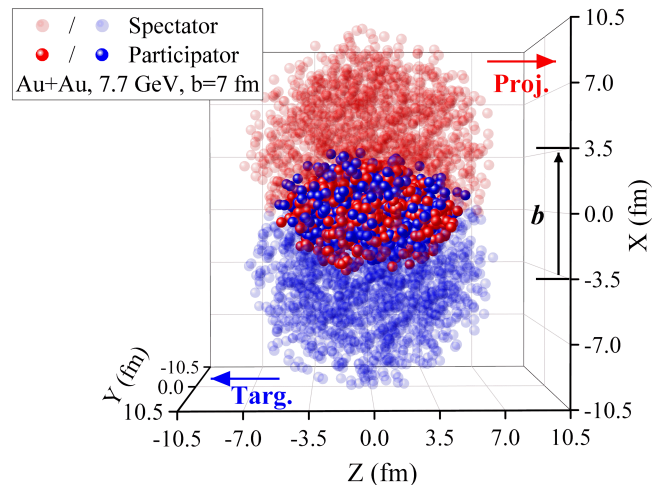


FIG. 1. The initial spatial distribution of nucleons in the impact parameter  $b = 7$  fm Au+Au collisions at  $\sqrt{s_{NN}} = 7.7$  GeV.

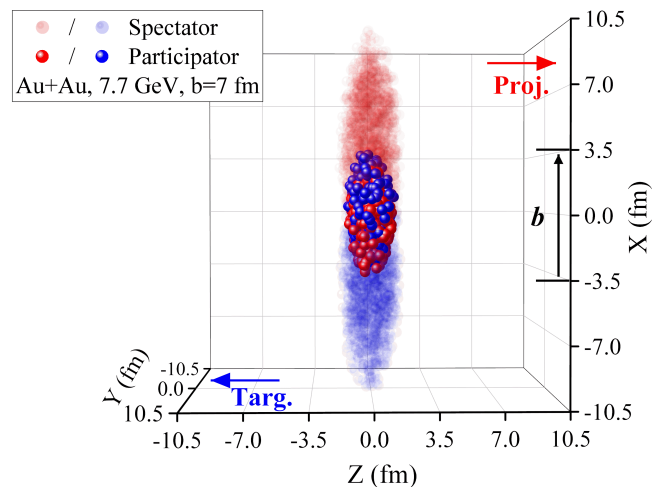


FIG. 2. The initial spatial distribution of nucleons in the impact parameter  $b = 7$  fm Au+Au collisions at  $\sqrt{s_{NN}} = 7.7$  GeV after Lorentz contraction.

hadronic state of the heavy-ion collision. The particle (nucleon or hadron) list is then updated by removing two colliding particles from the particle list and adding the generated particles to the particle list. Consequently, the  $NN$  ( $hh$ ) collision time list is updated by removing the  $NN$  ( $hh$ ) collision pair containing any one of the colliding particles from the old collision time list and adding the new collision pairs composed of one particle from the generated particles and another one from the old particle list.

A new  $NN$  ( $hh$ ) collision with least collision time is then selected from the updated collision time list and properly executed. With repeating the aforementioned steps until the particle collision time list is empty, a Monte Carlo simulation for a heavy-ion collision is finished.

<sup>1</sup> <https://github.com/ArcsaberHep/PACIAE>;  
<https://gitee.com/arcsaberhep/PACIAE>.

Therefore, in PACIAE model, a heavy-ion collision is indeed described as a Cumulative Superposition (CS) of the  $NN$  ( $hh$ ) collisions, i.e. the generated new hadrons will join in the processes of updating hadron list and  $hh$  collision time list, as shown in Fig. 3.

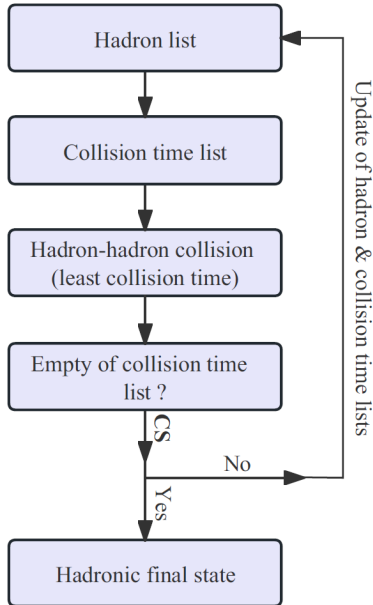


FIG. 3. A sketch for superposition of hadron-hadron collisions.

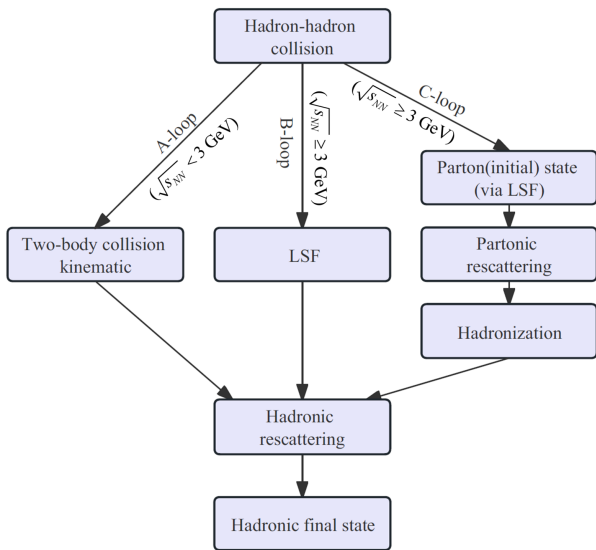


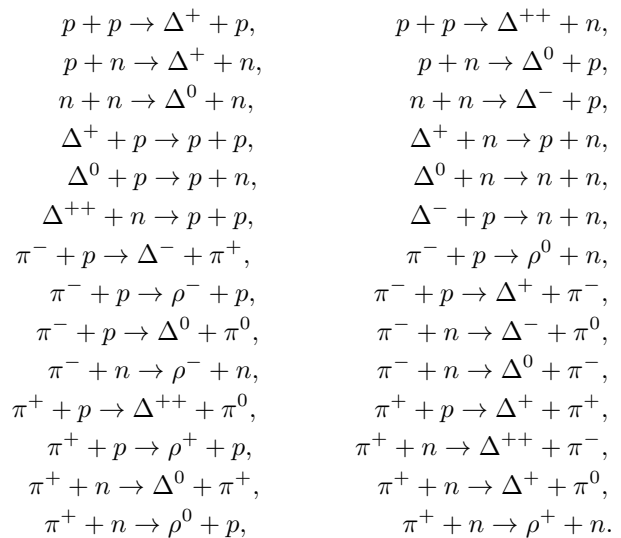
FIG. 4. A sketch of the hadron-hadron collision.

### III. MODEL FOR HADRON-HADRON COLLISION

The last section is common for the A-, B-, and C-simulation loops but leaves a problem of the  $hh$  collision execution. It will be addressed in this section for A-, B-, and C-loops, individually.

The  $hh$  collision in A-loop simulation is well described by the two-body elastic and inelastic scattering kinematics in hadronic degree of freedom [2], as shown in the left part of Fig. 4.

Upto the second time of updating collision list, the inelastic scattering is restricted to the following processes:



For both the elastic and inelastic scattering processes, the four momenta of scattered hadrons are determined by the energy-momentum conservation [10]. Among the inelastic scattering processes, if it is an exothermic reaction, such as  $p + p \rightarrow \Delta^+ + p$ , the threshold energy effect is taken into account. For an exothermic inelastic scattering, if the kinetic energy of its incident channel is less than the threshold energy, it should be dealt as an elastic scattering rather than inelastic scattering originally. Here two parameters are essential: One is the ratio of inelastic cross section to total cross section  $R_{inela/tot}$  ('x\_ratio' in program). Another is the  $\Delta$  particle instantaneously decay probability ('decpro') at the moment of formation.

Inspired by the additive quark model [31], we assume different outgoing channels and the resonance production process developed from a given incident channel are equally distributed. Upto the second time of updating collision list, there is only one resonance process of  $p + \pi^+ \rightarrow \Delta^{++}$  to be considered.

In PACIAE model, the experimental data of  $\sigma_{NN}^{tot} \approx 70$  mb measured at LHC energies and  $\sigma_{NN}^{tot} \approx 40$  mb measured at RHIC energy and below are adopted [32]. The total cross section of  $IJ$  collision (hadron  $I$  bombards with  $J$ ), is assumed to be proportional to the  $NN$

collision one, with the coefficient calculated by [2, 31]:

$$C_{IJ} = \frac{n_{eff}^I n_{eff}^J}{n_{eff}^N n_{eff}^N}, \quad (2)$$

$$n_{eff}^I = n_d^I + n_u^I + 0.6n_s^I + 0.2n_c^I + 0.07n_b^I. \quad (3)$$

In above equation the  $n_i^I$ , refers to the number of effective  $i$ -th valence quark (antiquark) in the  $I$ -th hadron.

Differently, in the high energy B-loop simulation the final hadronic state of a  $hh$  collision is supplied by PYTHIA [1]: As a proton consists of three valence quarks, countless sea quarks and gluons, a  $pp$  collision, may comprise  $n_{MPI}$  parton-parton pair interactions. Here  $n_{MPI}$  refers to the number of MultiParton Interactions (MPI). Each parton-parton collision is described by a Hard Scattering (HS) together with the Initial State Radiation (ISR, or initial state parton shower) and Final State Radiation (FSR, or final state parton shower). The resulted partons then hadronize together with two remnants providing the final hadronic state for a  $pp$  collision. Here the remnant refers to the left part of colliding proton, beside the ones join in the hard scattering. Fig 5 without PRS (Partonic ReScattering) and HRS (Hadronic ReScattering) is just a schematic diagram of the physical processes included in a  $pp$  collision.

The hadronization in PYTHIA model is phenomenologically described by the string iterative breaking processes: In case of the iterative string breaking process starts at the  $q_0$  end of a  $q_0\bar{q}_0$  string, if the string energy is large enough, a new  $q_1\bar{q}_1$  pair may be excited from the vacuum, such that a meson of  $q_0\bar{q}_1$  may formed and left behind the quark  $q_1$ . Later on,  $q_1$  quark in its turn may excite a  $q_2\bar{q}_2$  pair from the vacuum and combines another meson together with the  $\bar{q}_2$ . Repeating this breaking process, a lot of mesons are formed in the final hadronic state of the  $hh$  collision system, as shown in Fig. 6.

Fig. 7, taken from Ref. [2], shows the baryon (antibaryon) generation process in the popcorn model [2]: One starts from a red-antired ( $r\bar{r}$ ) string (with color flow indicated by the arrow in panel a). A green-antigreen ( $g\bar{g}$ ) pair may be excited from vacuum between  $r\bar{r}$  reversing the color flow in the central part of the string (panel b). A third blue-antiblue ( $b\bar{b}$ ) pair is created and breaks the string into two (panel c). Then another string breaking process happens and produces a  $b\bar{b}$  meson between the baryon ( $rgb$ ) and antibaryon ( $\bar{b}\bar{g}\bar{r}$ ).

Takeing meson production as an example, once the  $q_{i-1}$  and  $\bar{q}_i$  flavors are sampled, a selection should be made between the possible multiplets. The different multiplets have different relative composition probability, which is not given by first principle but must depend on the fragmentation processes, cf. [1] for the details.

In C-loop  $hh$  collision simulation, we first forcedly turn-off the hadronization before the execution of PYTHIA and break-up the strings and diquarks after

the execution of PYTHIA, resulting an initial partonic state. This partonic state then undergoes the partonic rescattering, where the lowest-order perturbative quantum chromodynamics (LO-pQCD) parton-parton interaction cross section [34, 35] is employed. After partonic rescattering the hadronization is implemented by the LUND string fragmentation regime and/or the coalescence model (see Sec. VIII). The hadronic rescattering is then followed, generating a final hadronic state for a  $hh$  collision system. Meanwhile, this simulation could be selected to stop at any stage desired conveniently. Fig. 5 shows the above physical processes in a C-loop  $pp$  simulation.

#### IV. PARTONIC RESCATTERING IN C-LOOP SIMULATION

In PACIAE model, the partonic rescattering is implemented in C-loop simulation and only  $2 \rightarrow 2$  processes are considered. The simulation framework of partonic rescattering is similar to that in the Sec. II: We first construct an initial parton-parton collision time list based on the parton list in the initial partonic state. Secondly, a parton-parton collision with least collision time is performed. Thirdly, the parton list and parton-parton collision time list are updated. A new parton-parton collision with least collision time is then selected from the updated collision time list and properly executed. With repeating the aforementioned steps until the parton-parton collision time list is empty, a Monte Carlo simulation for partonic rescattering is finished.

Table I gives the considered parton-parton interactions, where the differential cross section is expressed in the form of

$$\frac{d\sigma}{dt}(ab \rightarrow cd; s, t) = K \frac{\pi\alpha_s^2}{s^2} |\overline{M}(ab \rightarrow cd)|^2, \quad (4)$$

and calculated by the LO-pQCD approximation [34, 35]. In the equation above the  $\alpha_s$  refers to strong coupling factor. The  $s$ ,  $t$  and  $u$  (cf. Table I) are the Mandelstam invariants in the kinematics of  $ab \rightarrow cd$  quark process. And  $K$  is an enlarged factor introduced empirically. The corresponding integral cross section is

$$\frac{d\sigma}{dt}(ab \rightarrow cd; s) = \int_{-s}^0 \frac{d\sigma}{dt}(ab \rightarrow cd; s, t) dt. \quad (5)$$

As the differential cross section is divergent at  $t \rightarrow 0$ , Debye screening coefficient  $\mu$  has to be introduced. Therefore, taking the number 1 process in Table I as an example, its matrix element in differential cross section should be modified to

$$|M(q_1 q_2 \rightarrow q_1 q_2)|^2 = \frac{4}{9} \frac{s^2 + u^2}{t^2 - \mu^2}. \quad (6)$$

Among the listed parton-parton collisions in Table I, the number 1, 2, 3, 5, 8, and 9 processes are elastic

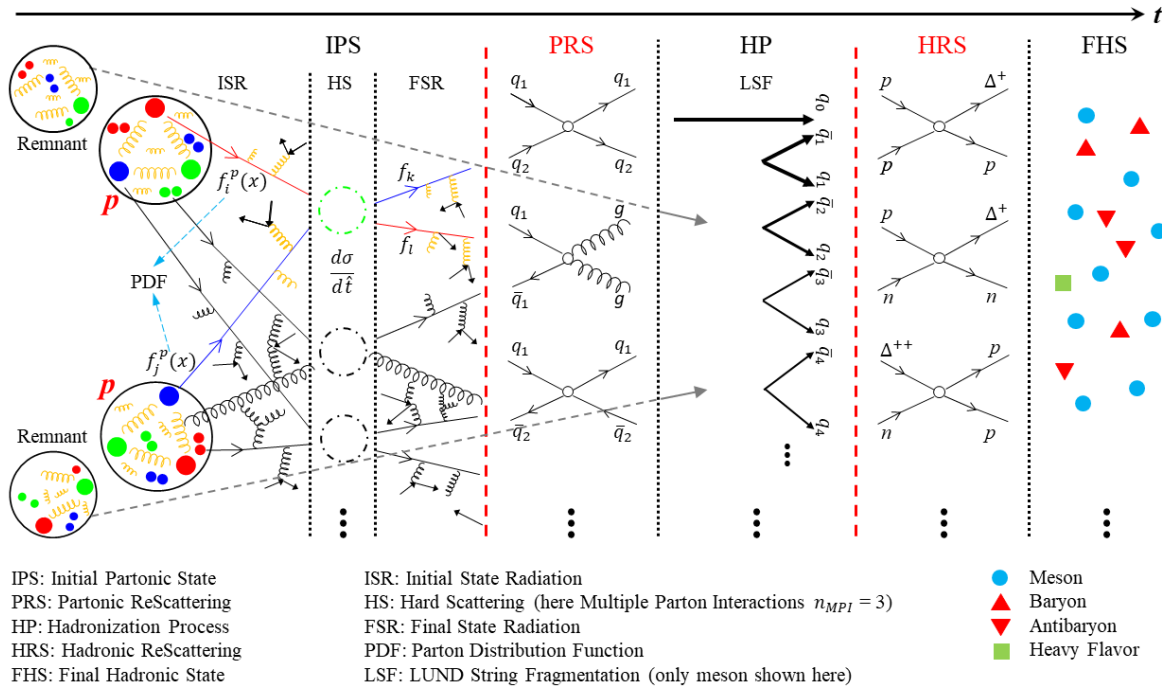


FIG. 5. A sketch for the physical routines in a high energy  $pp$  simulation.

TABLE I. Parton-parton collisions.

Order	Process	$ \overline{M} ^2$
1	$q_1 q_2 \rightarrow q_1 q_2$	$\frac{4}{9} \frac{s^2 + u^2}{t^2}$
2	$q_1 q_1 \rightarrow q_1 q_1$	$\frac{4}{9} \left( \frac{s^2 + u^2}{t^2} + \frac{s^2 + t^2}{u^2} \right) - \frac{8}{27} \frac{s^2}{ut}$
3	$q_1 \bar{q}_2 \rightarrow q_1 \bar{q}_2$	$\frac{4}{9} \frac{s^2 + u^2}{t^2}$
4	$q_1 \bar{q}_1 \rightarrow q_2 \bar{q}_2$	$\frac{4}{9} \frac{t^2 + u^2}{s^2}$
5	$q_1 \bar{q}_1 \rightarrow q_1 \bar{q}_1$	$\frac{4}{9} \left( \frac{s^2 + u^2}{t^2} + \frac{t^2 + u^2}{s^2} \right) - \frac{8}{27} \frac{u^2}{ts}$
6	$q\bar{q} \rightarrow gg$	$\frac{32}{27} \frac{u^2 + t^2}{ut} - \frac{8}{3} \frac{u^2 + t^2}{s^2}$
7	$gg \rightarrow q\bar{q}$	$\frac{1}{6} \frac{u^2 + t^2}{ut} - \frac{3}{8} \frac{u^2 + t^2}{s^2}$
8	$qq \rightarrow qq$	$-\frac{4}{9} \frac{u^2 + s^2}{us} + \frac{u^2 + s^2}{t^2}$
9	$gg \rightarrow gg$	$\frac{9}{2} \left( 3 - \frac{ut}{s^2} - \frac{us}{t^2} - \frac{st}{u^2} \right)$

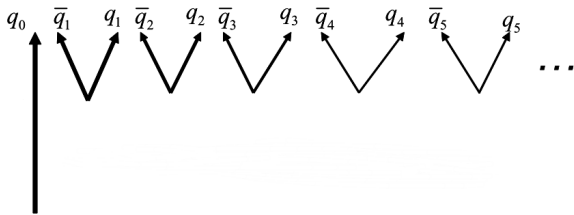


FIG. 6. The Feynman diagram like sketch for the string iterative breaking processes starting from the quark end of a  $q_0 \bar{q}_0$  string.

scattering processes. In the elastic scattering process, as quark flavors in incident and outgoing channels are unchanged, it is easy to handle. Most of the parton and hadron transport models, like AMPT [9] and the PACIAE 2.2, only take elastic parton-parton scattering processes into account. In PACIAE 3.0, the number 4, 6, and 7 inelastic parton-parton scattering processes are implemented.

In the number 4 and 7 inelastic scattering processes, if the invariant mass of incident channel is large enough, the available outgoing flavor may be different. We assume the different outgoing flavor is distributed inversely

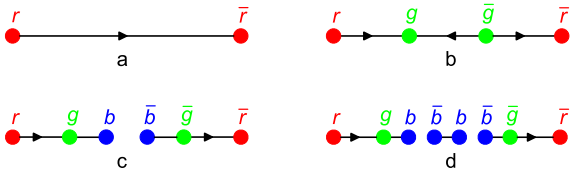


FIG. 7. The step-wise sketch illustrating the popcorn production of a baryon-antibaryon pair in the string iterative breaking processes, taken from [2].

proportional to the  $x$ -th power of its respective constituent quark mass ( $p_q \propto m_q^{-x}$ ). Here  $x$  is a parameter (default,  $D=3.65$ ).

## V. HADRONIC RESCATTERING

The simulation framework of hadronic rescattering is also similar to the one in the Sec. II. However, here we first filter out the desired hadrons from the available hadron list after hadronization to construct an initial hadron list. We then construct a hadronic collision time list, select a  $hh$  collision pair with least collision time and execute it properly, update hadron list and hadronic collision time list, etc., one step after another, like that in the Sec. II.

Here the  $NN$  total cross section is also taken from experiment and the total cross section of  $IJ$  incident channel is assumed to be proportional to the  $NN$  one with coefficient given by Eq. (2). The ratio of inelastic to total cross section ('x.ratio' in program,  $D=0.85$ ) is a model parameter, too.

In the hadronic rescattering we consider nearly 600 different inelastic  $hh$  collisions (cf. program packet hadcas.30.f), besides the elastic  $hh$  collision. The inelastic  $hh$  collisions listed at the begin of section III, for instance, are main parts of them. If user desired channel is not in the 600 list, it has to be added manually.

## VI. CENTRALITY DEFINITION AND EXPRESSION

In experiment, the centrality of a nucleus-nucleus ( $AB$ ) collision is usually defined as a percentile  $c$  in the  $AB$  total cross section and is assumed to be approximately equivalent to the fraction of charged particle multiplicity above a multiplicity cut of  $N_{ch}^{cut}$  [23]:

$$c \approx \frac{1}{N_{ch}^{tot}} \int_{N_{ch}^{cut}}^{N_{ch}^{tot}} d\sigma/dN_{ch}' dN_{ch}' \quad (7)$$

Meanwhile, this percentile  $c$  is also assumed to be equivalent to the fraction in impact parameter distri-

bution [10, 36]

$$c \approx \frac{2}{b_{max}^2} \int_0^b b' db' \quad (8)$$

Therefore a mapping relation

$$b = \sqrt{c} \times b_{max}, \quad (9)$$

is obtained [10, 23]. In the above equation  $b_{max}$  is defined as

$$b_{max} = R_A + R_B + 2 \times d, \quad (10)$$

where  $R_A$ , for instance, is given by

$$R_A = r_0 A^{1/3}, \quad r_0 = 1.12 fm. \quad (11)$$

Here  $A$  also denotes the atomic number of the nucleus.  $d = 0.546$  fm refers to the diffusivity parameter describing the tail of nuclear density profile.

In response to the observations from ALICE, ATLAS, and CMS that the maximum impact parameter should be extended to 20 fm, in PACIAE 3.0 we assume

$$b_{max} = R_A + R_B + f \times d. \quad (12)$$

The coefficient  $f$  is fixed by fitting the results of improved Monte Carlo Glauber model simulations [37]. It gives  $f \approx 4$  for the nucleus-nucleus collisions and  $f \approx 2$  for the proton-nucleus collisions [23]. Therefore we propose that, in the absence of experimental data on impact parameters, one can employ the Eqs. (9), (12) and fitted  $f$  value to calculate it.

In the heavy-ion collisions, the centrality is always represented by the number of participant nucleons  $N_{part}$ . It is calculated, in PACIAE model, by the optical Glauber model [10, 23, 38]. A relationship of

$$\langle T_{AA} \rangle = \frac{\langle N_{coll} \rangle}{\sigma_{NN}^{inel}}, \quad (13)$$

is employed to calculate the binary  $NN$  collision number  $N_{coll}$ . In the above equation  $T_{AA}$  is the nuclear overlap function and the angle bracket indicates averaging over events.

## VII. STRANGENESS ENHANCEMENT

In the string fragmentation picture of the relativistic  $NN$  and heavy-ion collisions, strange quark production is suppressed comparing to up and down quarks due to the tunneling probability [1]

$$P(m_{\perp q}) = \exp\left(-\frac{\pi}{\kappa} m_q^2\right) \exp\left(-\frac{\pi}{\kappa} p_{\perp q}^2\right), \quad (14)$$

where the  $\kappa \approx 1$  GeV/fm  $\approx 0.2$  GeV<sup>2</sup> is the (vacuum) string tension for a pure  $q\bar{q}$  string. However a pronounced enhancement of strange particle relative to pion production is really observed by ALICE collaboration in the

relativistic  $pp$  collisions [39]. To this end, we introduce an effective string tension stemming from single string structure [40] and the multiple string interaction [41, 42] instead of (vacuum) string tension in Eq. (14).

In Ref. [40], we have constructed a parameterized effective string tension coming from the single string structure:

$$\kappa_{eff}^s = \kappa_0(1 - \xi)^{-\alpha}. \quad (15)$$

In the above equation,  $\kappa_0$  is string tension of pure (dipole)  $q\bar{q}$  string.  $\alpha$  is a parameter to be tuned with experimental data.  $\xi$  is parameterized as:

$$\xi = \frac{\ln(\frac{k_{\perp max}^2}{s_0})}{\ln(\frac{s}{s_0}) + \sum_{j=gluon} \ln(\frac{k_{\perp j}^2}{s_0})}, \quad (16)$$

where  $k_{\perp}$  denotes the transverse momentum of the gluons inside a dipole string. The  $\sqrt{s}$  and  $\sqrt{s_0}$  give the mass of the string system and the parameter related to the typical hadron mass, respectively. The  $\xi$  quantifies the difference between a gluon wrinkled string and a pure  $q\bar{q}$  string. The value of this effective string tension changes on a string-by-string basis in the current implementation and takes the string-wise fluctuations into consideration.

Later on, we consider the multiple string interaction effects from the correlation of strings overlapping in a limited transverse space by parameterizing the effective string tension, in a manner similar to the close-packing strings discussed in Ref. [43] as follows:

$$\kappa_{eff}^m = \kappa_0 \left(1 + \frac{\frac{N_{coll}}{N_{part}} n_{MPI} - 1}{1 + p_{T,ref}^2/p_0^2}\right)^r. \quad (17)$$

In the above equation, the  $n_{MPI}$  indicates the number of multiple parton interactions in a  $pp$  collision system and  $p_{T,ref}^2/p_0^2$  shows the transverse scale of a typical string object relative to the proton size. The exponent  $r$  is then treated as a free parameter. As larger  $n_{MPI}$  leads to a denser string system in an event,  $n_{MPI}$  strongly correlates with the charged particle multiplicity. The factor of  $N_{coll}/N_{part}$  amplifies the multiple string interaction effects in heavy-ion collisions [42]. Multiplying  $\kappa_{eff}^s$  on both side of Eq. (17), one obtains

$$\begin{aligned} \kappa_{eff}^s \times \kappa_{eff}^m &= \kappa_{eff}^s \left(1 + \frac{\frac{N_{coll}}{N_{part}} n_{MPI} - 1}{1 + p_{T,ref}^2/p_0^2}\right)^r \\ &\equiv \kappa_{eff}^{s+m}. \end{aligned} \quad (18)$$

In PYTHIA [1] the strange quark suppression relevant parameters are:

- (1) PARJ(1), the suppression of diquark-antidiquark pair production in string-breaking process, compared with quark-antiquark pair production.
- (2) PARJ(2), the suppression of  $s$  quark pair production compared with  $u$  or  $d$  pair production.

(3) PARJ(3), the extra suppression of  $s$  diquark production compared with the normal suppression of  $s$  quarks.

(4) PARJ(21), Gaussian width of the transverse momentum distribution for primary hadrons in fragmentation.

They can be related to the effective string tension through a scaling function implied by the tunneling probability:

$$\lambda_2 = \lambda_1 \frac{\kappa_1^{eff}}{\kappa_2^{eff}}. \quad (19)$$

In the above equation,  $\kappa_1^{eff}=1$  GeV/fm represents the vacuum string tension and  $\kappa_2^{eff}$  is the effective string tension. The  $\lambda_1$  and  $\lambda_2$  refer to the one among PARJ(1), PARJ(2), and PARJ(3) before and after modification, respectively. The  $\lambda_2$  will be enlarged when the effective string tension  $\kappa_2^{eff}$  becomes greater than  $\kappa_1^{eff}$ .

Similarly, the PARJ(21) varies with the effective string tension as

$$\sigma_2 = \sigma_1 \left(\frac{\kappa_2^{eff}}{\kappa_1^{eff}}\right)^{1/2}. \quad (20)$$

## VIII. PHENOMENOLOGICAL COALESCENCE HADRONIZATION MODEL

There are two hadronization mechanisms implemented in C-loop simulation: The LUND string fragmentation regime and the coalescence (hadronization) model COCCNU (CO: the moral of coalescence, CCNU: the short of Central China Normal University). It is a phenomenological coalescence model unlike the semi-analytical coalescence models in Refs. [44–49].

In the PACIAE C-loop simulation, if coalescence model is selected, one then starts from the parton list (composed of quarks, antiquarks, and gluons) available after partonic rescattering. All the gluons in this parton list are randomly split into quark-antiquark pairs, resulting in a new parton list composed of quarks (antiquarks) only.

Then the collision system proceeds with energetic quark (antiquark) deexcitation process: A cycle over quark (antiquark) in the parton list is constructed. If the energy of a quark (antiquark) is larger than the deexcitation threshold energy  $e_{she}$ , it deexcites according to the vacuum excitation regime of  $q_0 \rightarrow q_0 q_1 \bar{q}_1$  ( $\bar{q}_0 \rightarrow \bar{q}_0 q_1 \bar{q}_1$ ) [1]. The generated quark-antiquark pair is filled at the end of the parton list. This deexcitation process is continuously repeated until the quark (antiquark) energy goes down to  $e_{she}$ . In each step, the transverse momenta of generated quark-antiquark pair are sampled according to the Gaussian or exponential distributions (controlled by parameter ‘i\_pT’). The generated quark-antiquark pair takes a part of its

mother quark (antiquark) energy, the fraction of this part is sampled randomly from an uniform distribution or fragmentation functions [1] (controlled by parameter ‘adj1(29)’). Of course, the corresponding four momentum should be subtracted from mother quark (antiquark). The finishing of this cycle presents the end of the first generation deexcitation, followed by the second generation deexcitation with a new cycle over the generated quarks (antiquarks). A free parameter ‘adj1(16)’ is set for the allowed maximum number of deexcitation generation (D=1).

In the gluon splitting and the energetic quark (antiquark) deexcitation processes, a key problem is the flavor generation probability of the outgoing channel. We assume the different outgoing flavors are distributed inversely proportional to the  $x$ -th power of their respective constituent quark masses. Here the  $x$  is a parameter. The  $x=1$  is assumed in [30] for the calculation of effective number of quarks in the hadron.

After the gluon splitting and the energetic quark (antiquark) deexcitation, the collision system is represented by a quark (antiquark) list. Then it proceeds to a combination loop: Selecting a proper quark and antiquark from the parton list to form a specific meson in the meson Table II, and/or choosing three quarks (antiquarks) to coalesce into a specific baryon (antibaryon) in the baryon Table III. Here many strategies are possible, for example, the combination starts from quark or antiquark, to combine into a meson or baryon, etc. Which one is better has to be decided by reproducing the experimental data. Presently, the combination starts from antiquark in PACIAE 3.0. An antiquark is assumed to form an antibaryon together with two other antiquarks by probability  $p = \frac{adj1(31)*adj1(33)}{1+adj1(31)*adj1(33)}$  and to form a meson together with a quark by probability  $(1-p)$ . adj1(31) and adj1(33) are two free parameters in the program. This combination loop is performed over the parton list until it is empty. If the empty of parton list is hard to reach, the remaining partons will attempt to re-hadronize by string fragmentation [1].

We assumes the three-momentum of the coalesced hadron is the sum of its constituent quark (antiquark) three-momentum. The extra energy (the part deviated from the conservation) is additionally counted into a specific array, left for sharing among partons and hadrons in the current list. The three-position of the coalesced hadron is the random summation of the three-position of its constituent quark (antiquark). The time of coalesced hadron is assumed to be the latest time among the constituent quarks (antiquarks).

Meanwhile, the phase space constraint

$$\frac{16\pi^2}{9}\Delta r^3\Delta p^3 = \frac{h^3}{d}, \quad (21)$$

is considered. In the above equation the  $h^3/d$  is the volume occupied by a single hadron in the phase space,  $d=4$  refers to the spin and parity degeneracies of the hadron. The  $\Delta r$  and  $\Delta p$  stand for the sum of pair-wise

relative distances between two (meson) or among three (baryon) partons in the spatial and momentum phase spaces, respectively.

The mesons and baryons considered are listed in Tables II and III, respectively. In the tables, the hadron proper probability is the expectation value (normalization factor) of its quark component wave function [50]. Only the hadron with nonzero proper probability can be the candidate in the coalescence hadronization. If the coalescing partons have the same possibility to form a pseudoscalar meson or a vector meson, (e.g.  $u\bar{d}$  can coalesce into a  $\pi^+$  or a  $\rho^+$ ) then the one with less mass discrepancy between the (invariant) mass of coalescing partons and the mass of hadron will be preferred. And the same is true for the baryon production.

## IX. COMPARISON WITH EXPERIMENTS

### A. High energy reaction

In B- and C-loop simulations, if the hadronization is implemented by LSF, the key parameters are  $K$ ,  $\sigma_G$ ,  $\alpha$ , and  $\beta$  (‘adj1(10)’, ‘adj1(34)’, ‘adj1(6)’ and ‘adj1(7)’ in PACIAE, corresponding to PARP(31), PARJ(21), PARJ(41) and PARJ(42) in PYTHIA).  $K$  is a multiplicative factor of hard scattering cross sections as shown in Eq. (4).  $\sigma_G$  is the width of Gaussian  $p_x$  and  $p_y$  transverse momentum distributions for the primary hadrons [1].  $\alpha$  and  $\beta$  are the parameters in the LUND fragmentation function [1, 51]:

$$f(z) \propto z^{-1}(1-z)^\alpha \exp(-\beta m_T^2/z), \quad (22)$$

where  $z$  is the fraction of energy taken by a hadron fragmented from a parton and  $m_T^2 = m^2 + p_T^2$  is transverse mass of the hadron. The  $\sigma_G$ ,  $\alpha$  and  $\beta$  hence couple with each other.

On the other hand, if the coalescence hadronization model (Coal) is selected in C-loop (note: B-loop is hadronized by LSF only), the key parameters would be  $K$ ,  $\sigma_q$ ,  $e_{she}$  (‘adj1(10)’, ‘adj1(34)’, and adj1(7)), and ‘adj1(16)’. Here  $K$  has the same meaning as mentioned above.  $\sigma_q$  and  $e_{she}$  are the width of excited quark-antiquark  $p_T$  in the energetic quark deexcitation and the threshold energy of deexcitation, respectively. The ‘adj1(16)’ refers to the allowed maximum number of deexcitation generation (D=1).

The midrapidity charged particle multiplicity density  $dN_{ch}/d\eta$  are given in Table. IV. Here we see the PACIAE model results well reproduce the experimental data from PHOBOS [52] and ALICE [53].

In Fig. 8, we compare the PHOBOS charged particle pseudorapidity distribution [54, 55] (black solid squares) measured in 0-6% most central Au+Au collisions at  $\sqrt{s_{NN}}=200$  GeV with B- and C-loop simulation results. The results of B-loop are indicated by red open squares, while the C-loop LSF and Coal are,



TABLE II. Mesons in coalescence hadronization model.

Quark conf.	Pseudoscalar Meson			Vector Meson		
	Name	Mass(GeV)	Proper probability	Name	Mass(GeV)	Proper probability
$u\bar{d}$	$\pi^+$	0.1396	1	$\rho^+$	0.7669	1
$d\bar{u}$	$\pi^-$	0.1396	1	$\rho^-$	0.7669	1
$u\bar{s}$	$K^+$	0.4936	1	$K^{*+}$	0.8921	1
$s\bar{u}$	$K^-$	0.4936	1	$K^{*-}$	0.8921	1
$d\bar{s}$	$K^0$	0.4977	1	$K^{*0}$	0.8962	1
$s\bar{d}$	$K^0$	0.4977	1	$\bar{K}^{*0}$	0.8962	1
$u\bar{u}$	$\pi^0$	0.1350	0.5	$\rho^0$	0.7700	0.5
$u\bar{u}$	$\eta$	0.5488	0.167	$\omega$	0.7820	0.5
$u\bar{u}$	$\eta'$	0.9575	0.333			
$d\bar{d}$	$\pi^0$	0.1350	0.5	$\rho^0$	0.7700	0.5
$d\bar{d}$	$\eta$	0.5488	0.167	$\omega$	0.7820	0.5
$d\bar{d}$	$\eta'$	0.9575	0.333			
$s\bar{s}$	$\eta$	0.5488	0.667	$\phi$	1.019	1
$s\bar{s}$	$\eta'$	0.9575	0.333			
$c\bar{d}$	$D^+$	1.869	1	$D^{*+}$	2.010	1
$d\bar{c}$	$D^-$	1.869	1	$D^{*-}$	2.010	1
$c\bar{u}$	$D^0$	1.865	1	$D^{*0}$	2.007	1
$u\bar{c}$	$\bar{D}^0$	1.865	1	$\bar{D}^{*0}$	2.007	1
$c\bar{s}$	$D_s^+$	1.969	1	$D_s^{*+}$	2.112	1
$s\bar{c}$	$D_s^-$	1.969	1	$D_s^{*-}$	2.112	1
$c\bar{c}$	$\eta_c$	2.980	1	$J/\Psi$	3.097	1
$u\bar{b}$	$B^+$	5.279	1	$B^{*+}$	5.325	1
$b\bar{u}$	$B^-$	5.279	1	$B^{*-}$	5.325	1
$d\bar{b}$	$B^0$	5.279	1	$B^{*0}$	5.325	1
$b\bar{d}$	$\bar{B}^0$	5.279	1	$\bar{B}^{*0}$	5.325	1
$s\bar{b}$	$B_s^0$	5.366	1	$B_s^{*0}$	5.415	1
$b\bar{s}$	$\bar{B}_s^0$	5.366	1	$\bar{B}_s^{*0}$	5.415	1
$c\bar{b}$	$B_c^0$	6.594	1	$B_c^{*0}$	6.602	1
$b\bar{c}$	$\bar{B}_c^0$	6.594	1	$\bar{B}_c^{*0}$	6.602	1
$b\bar{b}$	$\Upsilon$	9.460	1			

respectively, indicated by blue open circles and green open triangles. Fig. 9 is the same as Fig. 8 but for the transverse-momentum spectrum. In the simulations, the parameters were tuned as follows:

- (1) B-loop:  $K = 0.9, \sigma_G = 0.45, \alpha = 0.3, \beta = 0.58$ .
- (2) C-loop LSF:  $K = 2.5, \sigma_G = 0.45, \alpha = 0.3, \beta = 0.1$ , and  $\text{PARP}(82) = 2.5$ <sup>2</sup>.
- (3) C-loop Coal:  $K = 0.7, \sigma_q = 0.6, e_{she} = 1.8$ , and  $\text{PARP}(91) = 1.3$ <sup>3</sup>.

One can see in these two figures that the PACIAE model well reproduces the PHOBOS data within the error bars.

A similar comparison with ALICE data measured in 0-5% most central Pb+Pb collisions at  $\sqrt{s_{NN}} = 2.76$  TeV is shown in Figs. 10 and 11. The parameters are:

- (1) B-loop:  $K = 2.9, \sigma_G = 0.6, \alpha = 0.3, \beta = 0.13$ .
- (2) C-loop LSF:  $K = 2.9, \sigma_G = 0.6, \alpha = 0.3, \beta = 0.012$ .
- (3) C-loop Coal:  $K = 1.5, \sigma_q = 0.6, e_{she} = 1.9$ , and  $\text{PARP}(91) = 0.6$ .

Figs. 10 and 11 show that, PACIAE model gives good descriptions to the ALICE charged particle pseudorapidity distribution [56] and  $p_T$  distribution data [57], except that the  $p_T$  distribution from ‘‘C-loop Coal’’ is slightly harder at  $p_T > 4$  GeV/c region.

<sup>2</sup> The regularization scale of transverse-momentum spectrum for multiple interactions, parameter  $\text{parp82}$  in PACIAE.

<sup>3</sup> The width of primordial transverse momentum  $k_\perp$  for the partons inside the beam hadrons, parameter  $\text{adj1}(39)$  in PACIAE.

TABLE III. Baryons in coalescence hadronization model.

Quark conf.	Spin-Parity $\frac{1}{2}^+$			Spin-Parity $\frac{3}{2}^+$		
	Name	Mass(GeV)	Proper probability	Name	Mass(GeV)	Proper probability
<i>ddd</i>				$\Delta^-$	1.234	1
<i>ddu</i>	<i>n</i>	0.9396	1	$\Delta^0$	1.233	1
<i>duu</i>	<i>p</i>	0.9383	1	$\Delta^+$	1.232	1
<i>uuu</i>				$\Delta^{++}$	1.231	1
<i>dds</i>	$\Sigma^-$	1.197	1	$\Sigma^{*-}$	1.387	1
<i>dus</i>	$\Lambda^0$	1.116	0.5			
<i>dus</i>	$\Sigma^0$	1.193	0.5	$\Sigma^{*0}$	1.384	1
<i>uus</i>	$\Sigma^+$	1.189	1	$\Sigma^{*+}$	1.383	1
<i>dss</i>	$\Xi^-$	1.321	1	$\Xi^{*-}$	1.535	1
<i>uss</i>	$\Xi^0$	1.315	1	$\Xi^{*0}$	1.532	1
<i>sss</i>				$\Omega^-$	1.672	1
<i>ddc</i>	$\Sigma_c^0$	2.454	1	$\Sigma_c^{*0}$	2.518	1
<i>duc</i>	$\Lambda_c^+$	2.284	0.5			
<i>duc</i>	$\Sigma_c^+$	2.4535	0.5	$\Sigma_c^{*+}$	2.500	1
<i>dsc</i>	$\Xi_c^0$	2.4703	0.5			
<i>dsc</i>	$\Xi_c'^0$	2.550	0.5	$\Xi_c^{*0}$	2.630	1
<i>usc</i>	$\Xi_c^+$	2.4656	0.5			
<i>usc</i>	$\Xi_c'^+$	2.550	0.5	$\Xi_c^{*+}$	2.630	1
<i>uuc</i>	$\Sigma_c^{++}$	2.4529	1	$\Sigma_c^{*++}$	2.500	1
<i>dcc</i>	$\Xi_{cc}^+$	3.598	1	$\Xi_{cc}^{*+}$	3.6565	1
<i>ucc</i>	$\Xi_{cc}^{++}$	3.598	1	$\Xi_{cc}^{*++}$	3.6565	1
<i>ssc</i>	$\Omega_c^0$	2.704	1	$\Omega_c^{*0}$	2.800	1
<i>scc</i>	$\Omega_{cc}^0$	3.7866	1	$\Omega_{cc}^{*0}$	3.8247	1
<i>ccc</i>				$\Omega_{ccc}^{*+}$	4.9159	1
<i>ddb</i>	$\Sigma_b^-$	5.800	1	$\Sigma_b^{*-}$	5.810	1
<i>uub</i>	$\Sigma_b^+$	5.800	1	$\Sigma_b^{*+}$	5.810	1
<i>dub</i>	$\Sigma_b^0$	5.800	0.5	$\Sigma_b^{*0}$	5.810	1
<i>dub</i>	$\Lambda_b^0$	5.641	0.5			1
<i>dsb</i>	$\Xi_b^-$	5.840	0.5			
<i>dsb</i>	$\Xi_b'^-$	5.960	0.5	$\Xi_b^{*-}$	5.970	1
<i>usb</i>	$\Xi_b^0$	5.840	0.5			
<i>usb</i>	$\Xi_b'^0$	5.960	0.5	$\Xi_b^{*0}$	5.970	1
<i>dcb</i>	$\Xi_{bc}^0$	7.0057	0.5			
<i>dcb</i>	$\Xi_{bc}'^0$	7.0372	0.5	$\Xi_{bc}^{*0}$	7.0485	1
<i>ucb</i>	$\Xi_{bc}^+$	7.0057	0.5			
<i>ucb</i>	$\Xi_{bc}'^+$	7.0372	0.5	$\Xi_{bc}^{*+}$	7.0485	1
<i>dbb</i>	$\Xi_{bb}^-$	10.4227	1	$\Xi_{bb}^{*-}$	10.4414	
<i>ubb</i>	$\Xi_{bb}^0$	10.4227	1	$\Xi_{bb}^{*0}$	10.4414	
<i>ssb</i>	$\Omega_b^-$	6.120	1	$\Omega_b^{*-}$	6.130	1
<i>scb</i>	$\Omega_{bc}^0$	7.191	0.5			1
<i>scb</i>	$\Omega_{bc}'^0$	7.211	0.5	$\Omega_{bc}^{*0}$	7.219	1
<i>sbb</i>	$\Omega_{bb}^-$	10.6021	1	$\Omega_{bb}^{*-}$	10.6143	1
<i>ccb</i>	$\Omega_{bcc}^+$	8.3095	1	$\Omega_{bcc}^{*+}$	8.3133	1
<i>cbb</i>	$\Omega_{bbc}^0$	11.7077	1	$\Omega_{bbc}^{*0}$	11.7115	1
<i>bbb</i>				$\Omega_{bbb}^{*-}$	15.1106	1

### B. Low energy reaction

In the PACIAE A-loop simulation there are two parameters only. One is the ratio of the inelastic to to-

tal cross section  $R_{inela/tot}$  ('x\_ratio' in program), another is the instantaneous decay probability of  $\Delta$  particle ('decpro' in program). The  $R_{inela/tot}$  is assumed to

TABLE IV. The midrapidity charged particle multiplicity density  $dN_{ch}/d\eta$  in 0-6% most central Au+Au collisions at  $\sqrt{s_{NN}} = 0.2$  TeV for  $|\eta| < 1$  from PHOBOS [52] and 0-5% most central Pb+Pb collisions at  $\sqrt{s_{NN}} = 2.76$  TeV for  $|\eta| < 0.5$  from ALICE [53] compared with the results from PACIAE 3.0 B-loop, C-loop LSF and C-loop Coal.

System	$\sqrt{s_{NN}}$ (TeV)	Exp.	B-Loop	C-loop LSF	C-loop Coal
Au+Au	0.2	$1310 \pm 69$ <sup>a</sup>	1283	1301	1288
Pb+Pb	2.76	$1610 \pm 60$ <sup>b</sup>	1667	1672	1587

<sup>a</sup> Taken from PHOBOS [52]

<sup>b</sup> Taken from ALICE [53]

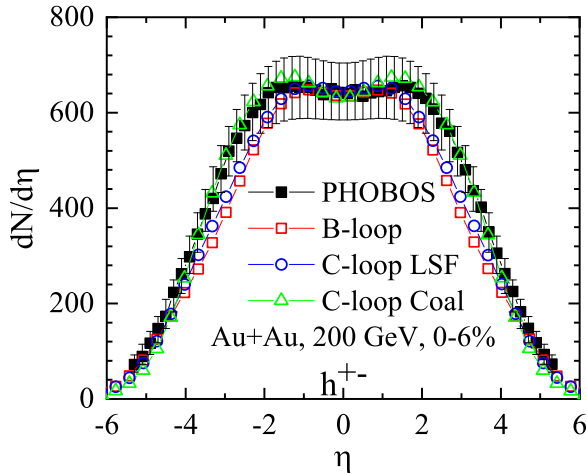


FIG. 8. (Color online) Charged particle pseudorapidity distribution in 0-6% most central Au+Au collisions at  $\sqrt{s_{NN}} = 200$  GeV from PACIAE model simulations comparing with PHOBOS data [54].

be a function of the incident channel  $\sqrt{s_{NN}}$  [58, 59]:

$$R_{inela/tot} = \frac{1.35(\sqrt{s_{NN}} - 2.015)^2}{0.015 + (\sqrt{s_{NN}} - 2.015)}, \text{ if } \sqrt{s_{NN}} < 3 \text{ GeV.} \quad (23)$$

In Fig. 12, we compare PACIAE simulated results (depro=0.9) of  $\pi^+$  and  $\pi^-$  yields to the corresponding FOPI experimental data [60] in most central Au+Au collisions at beam energy (fixed target) of 0.40, 0.60, 0.80, 1.0, 1.2, and 1.5A GeV (corresponding to  $\sqrt{s_{NN}}$  equal to 2.066, 2.155, 2.241, 2.402, and 2.520A GeV, respectively). Here one sees the results of PACIAE model well reproduce the experimental data.

The PACIAE model results of  $\pi^+/p$  and  $\pi^-/p$  ratios are shown in Fig. 13 and compared with FOPI experimental data measured in the same collision system like Fig. 12. Since in the final hadronic state generated in the PYTHIA (PACIAE) model the light nuclei (d, t,  $^3\text{He}$ ,  $^4\text{He}$ , Li, etc.) are not identified. The charge number of above light nuclei must first be added into the proton data and then compared with PACIAE results due to the charge conservation principle. Fig. 13 shows the PACIAE results reproduce the FOPI experimental data generally well.

The E895 measured  $\pi^+$  and  $\pi^-$  rapidity distribu-

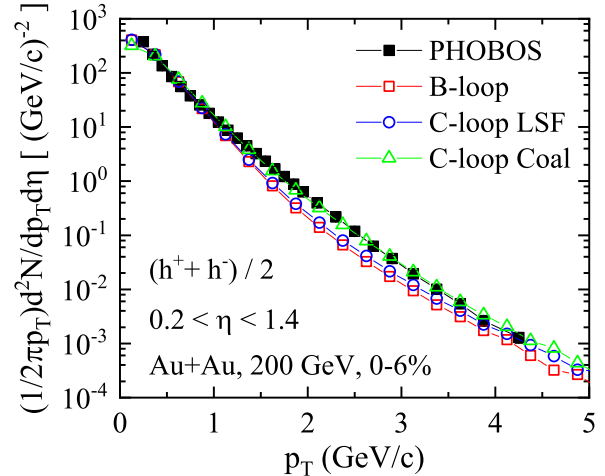


FIG. 9. (Color online) Charged particle invariant transverse momentum spectra in 0-6% most central Au+Au collisions at  $\sqrt{s_{NN}} = 200$  GeV from PACIAE simulations comparing with PHOBOS data [55].

tions [61] in 0-5% most central Au+Au collisions at nominal beam energy of 2 GeV/nucleon are compared with PACIAE results in Fig. 14. The actual beam energy after correction for the energy loss is 1.85A GeV, which is corresponding to  $\sqrt{s_{NN}} = 2.64$  GeV. One can see here the E895 measured  $\pi^+$  and  $\pi^-$  rapidity distributions are fairly well reproduced by PACIAE.

Similarly, Fig. 15 gives the comparison of E895 measured  $\pi^+$  and  $\pi^-$  transverse mass (transverse momentum) distributions [61] to the PACIAE results in the same collision system like Fig. 14. One can see here the experimentally measured  $\pi^+$  and  $\pi^-$  transverse mass distributions are harder than PACIAE simulations in the transverse mass interval of 0.1-0.3  $\text{GeV}/c^2$ , otherwise softer than PACIAE results. As the outgoing particle momentum in low energy A-loop simulation is fixed by the two-body scattering kinematic, and there are no adjustable parameters unlike that in the high energy B- and C-loop simulations, the improvement of the agreement between experiment and theory in particle transverse mass distribution has to be studied further.

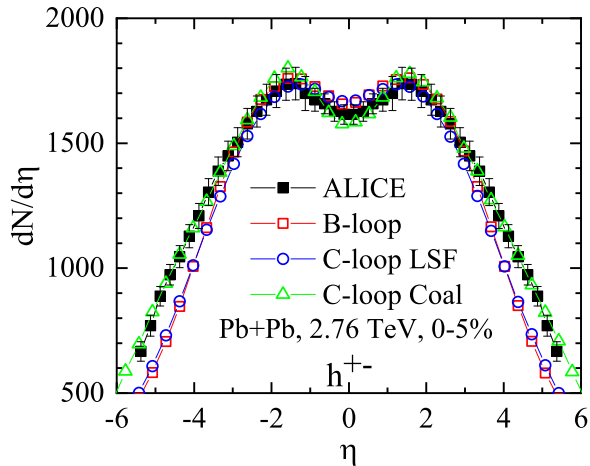


FIG. 10. (Color online) Charged particle pseudorapidity distribution in 0-5% most central Pb+Pb collisions at  $\sqrt{s_{NN}} = 2.76$  TeV from PACIAE simulations comparing with ALICE data [56].

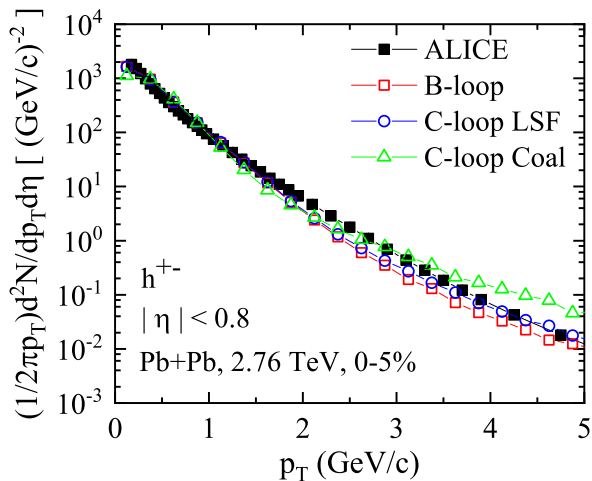


FIG. 11. (Color online) Charged particle invariant transverse momentum spectra in 0-5% most central Pb+Pb collisions at  $\sqrt{s_{NN}} = 2.76$  TeV from PACIAE simulations comparing with ALICE data [57].

## X. CONCLUSION

We have constructed a phenomenological parton and hadron cascade model PACIAE 3.0 based on PYTHIA 6.428 and PACIAE 2.2 series. The C-, B- and A-loop simulations are designed for the high and low energy nuclear collisions, respectively. In C-loop simulation, the parton-parton inelastic scatterings are implemented. The single string structure and multiple string interaction mechanisms are involved in the high energy B- and C-loop simulations for the strangeness enhancement investigation. An improved mapping formula between the percentage and impact parameter centrality definitions is proposed responding the ALICE, ATLAS, and CMS

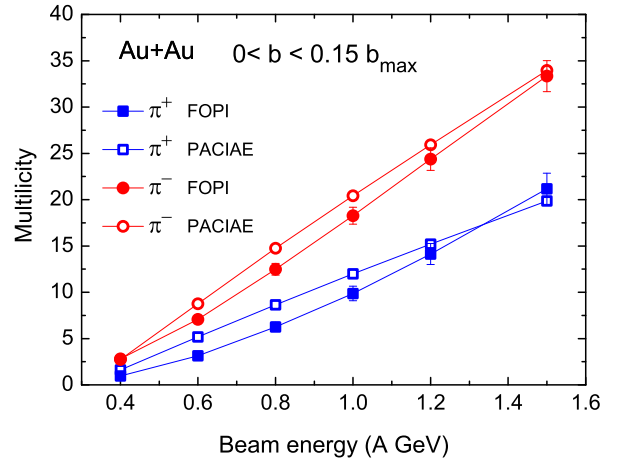


FIG. 12. (Color online) The  $\pi^+$  and  $\pi^-$  yields in most central Au+Au collisions at beam energy of 0.40, 0.60, 0.80, 1.0, 1.2, and 1.5A GeV from PACIAE model simulations comparing with the corresponding FOPI experimental data [60].

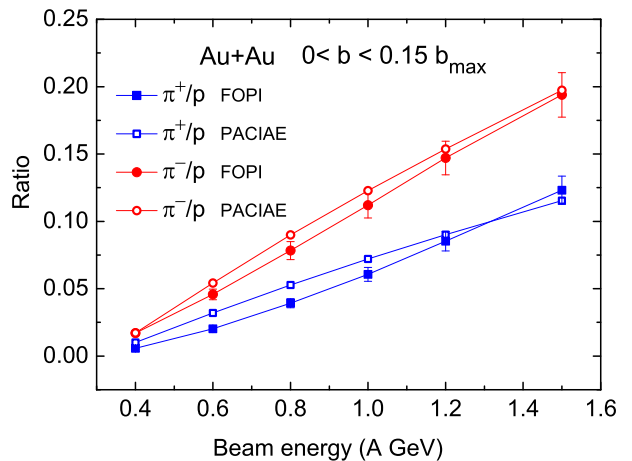


FIG. 13. (Color online) The  $\pi^+/p$  and  $\pi^-/p$  ratios in most central Au+Au collisions at beam energy of 0.40, 0.60, 0.80, 1.0, 1.2, and 1.5A GeV from PACIAE model simulations comparing with the FOPI experimental data [60].

observation of  $b_{max} \approx 20$  fm. The phenomenological coalescence hadronization model is also extensively modified in the C-loop simulation.

The simulated results are compared with the experimental data measured in FOPI and E895 experiments, and at RHIC as well as LHC energies, respectively. Generally speaking, the basic experimental data of particle yield, transverse momentum distribution, and the pseudorapidity distribution are reasonably reproduced.

It seems necessary to introduce the mean field, Fermi motion, and Pauli blocking effects in the A-loop simulation for the study of symmetry energy and the equation

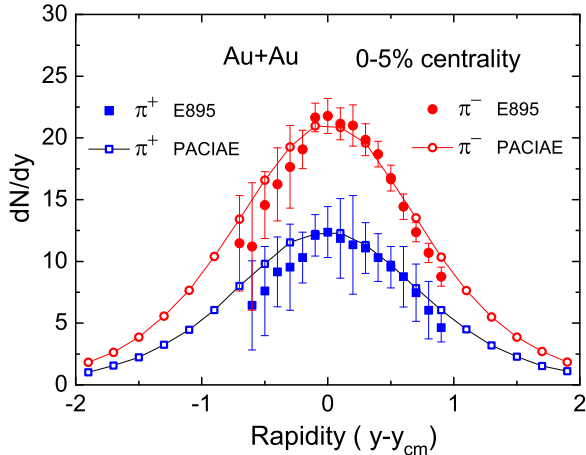


FIG. 14. (Color online) The E895  $\pi^+$  and  $\pi^-$  experimental rapidity distributions in 0-5% most central Au+Au collisions at 1.85A GeV actual beam energy [61] comparing with PACIAE model simulations.

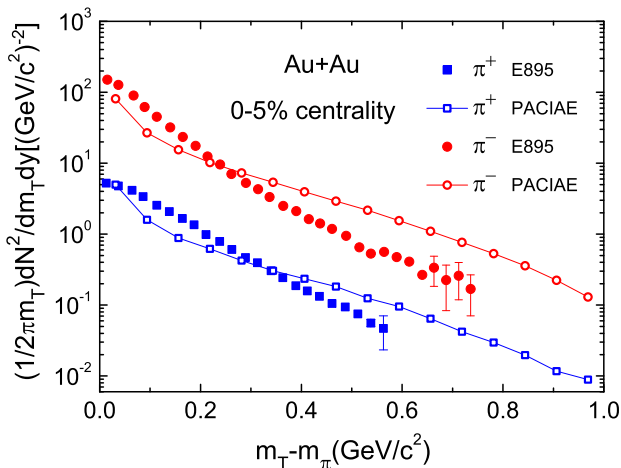


FIG. 15. (Color online) The same as the Fig. 14 but for  $\pi^+$  and  $\pi^-$  transverse mass distributions.

of state. For the investigation of heavy flavor production in relativistic nuclear collisions with B- and/or C-loop simulations, it may be obliged to open the special channels for ‘Heavy flavours’ sector in PYTHIA. It is a bias sampling method, the calculated results must be multiplied by a correcting (normalization) factor before comparison with experimental data.

At last, from a technical point of view, PACIAE 3.0 is written in FORTRAN programming language and based on PYTHIA 6. With the development of physics and computer science, high-energy community embraces more modern languages and technologies, in particular from FORTRAN to object-oriented C++ language. A plan of accessing to C++-based PYTHIA 8 [2] is one of

our future goals and is on the timetable, in which we expect more fruitful physics to be integrated with PACIAE.

## ACKNOWLEDGEMENTS

The author An-Ke Lei thanks Xiao-Ming Zhang, Shu-Su Shi, and Wen-Chao Zhang for helpful discussions. This work was supported by the National Natural Science Foundation of China (Grants Nos.: 12375135, 11775094, 11905188, 12275322) and the 111 project of the foreign expert bureau of China. Yu-Liang Yan acknowledges the financial support from Key Laboratory of Quark and Lepton Physics in Central China Normal University (Grant No. QLPL201805) and the Continuous Basic Scientific Research Project (Grant No. WDJC-2019-13).

## Appendix A: PACIAE 3.0 user’s guide

### 1. Program running

To run PACIAE 3.0, one direct way is to compile the source code, modify the input file “usu.dat” as needed, and execute the program. Another way is to use the toy SHELL-script “PACIAE.sh”. A Makefile has been integrated in the “PACIAE.sh” with GFortran compiler specified. It will compile the source code, generate “usu.dat” (the old “usu.dat” will be overwritten) and run the program automatically. More details could be found in “README.md” file.

PACIAE 3.0 comes with a simple internal on-line analyzing module and outputs several files. The analyzing output file is “rms.out”, where some basic results of collisions and six distributions (rapidity distribution  $dN/dy$ , invariant transverse momentum spectrum  $1/p_T dN/dp_T$ , pseudorapidity distribution  $dN/d\eta$ , invariant transverse mass spectrum  $1/m_T dN/dm_T$ , event-wise multiplicity distribution, and transverse momentum spectrum  $dN/dp_T$ ) are provided. The “rms0.out” is a file recording the input parameters. The “main.out” file is PYTHIA-style particle list output file. If user chooses to output OSCAR-format file, there will be an “oscar.out” file that records list of final state particles or full event history.

### 2. The basic tuning criteria

In Sec. IX, we have given rough tuning results at both low- and high-energies. A “tune” essentially requires a very large amount of experimental data fitting with a couple of adjustment parameters, such as the Perugia 2011 tune of PYTHIA 6 [62] and Monash 2013 tune of PYTHIA 8 [63] the ALICE typically used. However, for heavy-ion collisions, it is impossible to meet a “perfect”

tune due to our inadequate understanding of this very sophisticated large system. A recommended effective tuning criterion is: Fit the midrapidity density, pseudorapidity distributions and/or transverse momentum spectra of basic charged particles to the experimental data at the corresponding system and energy. Then one could conduct other studies of interest. Another criterion is based on what one would like to study. For instance, to study the topic of nuclear modification factors  $R_{AA}$ , one can fit the  $R_{AA}$  of  $\pi^\pm$  to experimental data at first [64].

### 3. Incident channel selection in the update of $hh$ collision list

The particle yield in final hadronic state is sensitively depended on the selection of incident channel in the update of  $hh$  collision list after each  $hh$  collision. Presently,

only the  $NN$  collision is selected at the beginning of  $hh$  simulation loop and in the subroutine of ‘updtlp’, ‘updatl’, and ‘intdis’ consistently, in the B- and C-loop simulations. In A-loop simulation, only the  $NN$ ,  $\Delta N$ , and  $\pi N$  are selected at the beginning of  $hh$  collision simulation loop and in the subroutine of ‘updatl\_nn’ and ‘intdis’ consistently.

### 4. Main switches and parameters

In the follows we list main switches and parameters as well as their potentials, respectively, for user reference. As mentioned above the ‘decpro’ and ‘x\_ratio’ are the only two free parameters in the A-loop simulation, thus the following Table V is just for the B- and C-loop simulations only. More details could be found in “usu.dat”, “PACIAE.sh”, and the comments in “main\_30.f”.

- 
- [1] T. Sjostrand, S. Mrenna, and P. Z. Skands, *J. High Energy Phys.* **05**, 026 (2006).
  - [2] C. Bierlich *et al.*, *SciPost Phys. Codebases* **8**, (2022).
  - [3] G. Corcella, I. G. Knowles, G. Marchesini, S. Moretti, K. Odagiri, P. Richardson, M. H. Seymour, and B. R. Webber, *J. High Energy Phys.* **01**, 010 (2001).
  - [4] T. Gleisberg, S. Hoeche, F. Krauss, M. Schonherr, S. Schumann, F. Siegert, and J. Winter, *J. High Energy Phys.* **02**, 007 (2009).
  - [5] K. Geiger and B. Muller, *Nucl. Phys. B* **369**, 600 (1992).
  - [6] X.-N. Wang and M. Gyulassy, *Phys. Rev. D* **44**, 3501 (1991).
  - [7] N. S. Amelin, L. V. Bravina, L. P. Csernai, V. D. Toneev, K. K. Gudima, and S. Y. Sivoklov, *Phys. Rev. C* **47**, 2299 (1993).
  - [8] S. A. Bass *et al.*, *Prog. Part. Nucl. Phys.* **41**, 255 (1998).
  - [9] Z.-W. Lin, C. M. Ko, B.-A. Li, B. Zhang, and S. Pal, *Phys. Rev. C* **72**, 064901 (2005).
  - [10] B.-H. Sa, D.-M. Zhou, Y.-L. Yan, X.-M. Li, S.-Q. Feng, B.-G. Dong, and X. Cai, *Comput. Phys. Commun.* **183**, 333 (2012).
  - [11] A. Kisiel, T. Taluc, W. Broniowski, and W. Florkowski, *Comput. Phys. Commun.* **174**, 669 (2006).
  - [12] W. Cassing and E. L. Bratkovskaya, *Nucl. Phys. A* **831**, 215 (2009).
  - [13] T. Pierog, I. Karpenko, J. M. Katzy, E. Yatsenko, and K. Werner, *Phys. Rev. C* **92**, 034906 (2015).
  - [14] J. Weil *et al.* (SMASH), *Phys. Rev. C* **94**, 054905 (2016).
  - [15] K. Kauder (JETSCAPE), *Nucl. Phys. A* **982**, 615 (2019).
  - [16] C. Bierlich, G. Gustafson, L. Lönnblad, and H. Shah, *J. High Energy Phys.* **10**, 134 (2018).
  - [17] Y.-X. Zhang *et al.* (TMEP), *Phys. Rev. C* **97**, 034625 (2018).
  - [18] H. Wolter *et al.* (TMEP), *Prog. Part. Nucl. Phys.* **125**, 103962 (2022).
  - [19] G.-C. Yong, *Phys. Rev. C* **96**, 044605 (2017).
  - [20] D.-M. Zhou, Y.-L. Yan, X.-L. Li, X.-M. Li, B.-G. Dong, X. Cai, and B.-H. Sa, *Comput. Phys. Commun.* **193**, 89 (2015).
  - [21] Y.-L. Yan, D.-M. Zhou, X. Cai, and B.-H. Sa, *Comput. Phys. Commun.* **224**, 417 (2018).
  - [22] Z.-L. She, D.-M. Zhou, Y.-L. Yan, L. Zheng, H.-g. Xu, G. Chen, and B.-H. Sa, *Comput. Phys. Commun.* **274**, 108289 (2022).
  - [23] Y.-L. Yan, D.-M. Zhou, A.-K. Lei, X.-M. Li, X.-M. Zhang, L. Zheng, G. Chen, X. Cai, and B.-H. Sa, *Comput. Phys. Commun.* **284**, 108615 (2023).
  - [24] B. H. Sa and A. Tai, *Comput. Phys. Commun.* **90**, 121 (1995).
  - [25] A. Tai and B.-H. Sa, *Comput. Phys. Commun.* **116**, 353 (1999).
  - [26] B. Andersson, A. Tai, and B.-H. Sa, *Z. Phys. C* **70**, 499 (1996).
  - [27] B.-H. Sa, X. Cai, A. Tai, and D.-M. Zhou, *Phys. Rev. C* **66**, 044902 (2002).
  - [28] H. Pi, *Comput. Phys. Commun.* **71**, 173 (1992).
  - [29] T. Sjostrand, *Comput. Phys. Commun.* **82**, 74 (1994).
  - [30] T. Sjöstrand and M. Utheim, *Eur. Phys. J. C* **80**, 907 (2020).
  - [31] E. M. Levin and L. L. Frankfurt, *JETP Lett.* **2**, 65 (1965).
  - [32] S. Acharya *et al.* (ALICE), ALICE-PUBLIC-2018-011, (2018).
  - [33] B.-H. Sa, D.-M. Zhou, Y.-L. Yan, B.-G. Dong, and X. Cai, *Comput. Phys. Commun.* **184**, 1476 (2013).
  - [34] B. L. Combridge, J. Kripfganz, and J. Ranft, *Phys. Lett. B* **70**, 234 (1977).
  - [35] R. D. Field, *Applications Of Perturbative QCD* (Addison-Wesley Publishing Company, Inc., New York, 1989).
  - [36] W. Broniowski and W. Florkowski, *Phys. Rev. C* **65**, 024905 (2002).
  - [37] C. Loizides, J. Kamin, and D. d’Enterria, *Phys. Rev. C* **97**, 054910 (2018), [Erratum: *Phys.Rev.C* 99, 019901 (2019)].
  - [38] K. J. Eskola, K. Kajantie, and J. Lindfors, *Nucl. Phys. B* **323**, 37 (1989); D. Miskowiec, <http://www-linux.gsi.de/~misko/overlap>.
  - [39] J. Adam *et al.* (ALICE), *Nature Phys.* **13**, 535 (2017).

TABLE V. Object of study vs. switch and/or parameter.

Simulation mode	iMode <sup>a</sup> = 1: A-loop ; =2: B-loop ; =3: C-loop.
QCD sub-processes selection	nchan = 0: inelastic (INEL); = 1: non-single diffractive (NSD); = 2: Drell-Yan; = 3: $J/\Psi$ production; = 4: heavy-flavor production; = 5: direct photon; = 6: soft only; = 7: $W^{+/-}$ production; = 8: default PYTHIA; = 9: $Z^0$ production.
Chiral magnetic effect	adj1(3)=0: off; =1, on.
Hadronization model	adj1(12) = 0: string fragmentation model; = 1: coalescence model.
Parton rescattering	adj1(1) > 0: with; = 0: without. adj1(1) is a factor multiplying on parton-parton cross section.
Process in parton rescattering	iparres = 0: elastic processes only; = 1: elastic + inelastic processes. i_inel_proc = 6: with inelastic process of 4, 6, and 7; = 7: with inelastic process 7 only.
String fragmentation model	adj1(10): K factor, adj1(6): $\alpha$ , adj1(7): $\beta$ , adj1(34): $\sigma_H$ .
Coalescence model	adj1(16): allowed number of deexcitation generation, adj1(17): threshold energy of deexcitation, adj1(29): deexcitation function, adj1(34): $\sigma_q$ .
Effective string tension	kjp22 = 1: variable single string tension; = 2: variable multiple string tension; = 3: variable single + multiple string tension; = 4: constant string tension.
Hadron rescattering	kjp21 = 1: with; =0: without.

<sup>a</sup> name in program (the same later)

- [40] A. Tai and B.-H. Sa, *Phys. Lett. B* **409**, 393 (1997).  
[41] L. Zheng, D.-M. Zhou, Z.-B. Yin, Y.-L. Yan, G. Chen, X. Cai, and B.-H. Sa, *Phys. Rev. C* **98**, 034917 (2018).  
[42] D.-M. Zhou, L. Zheng, Z.-H. Song, Y.-L. Yan, G. Chen, X.-M. Li, X. Cai, and B.-H. Sa, *Phys. Rev. C* **102**, 044903 (2020).  
[43] N. Fischer and T. Sjöstrand, *J. High Energy Phys.* **01**, 140 (2017).  
[44] R. C. Hwa and C. B. Yang, *Phys. Rev. C* **67**, 034902 (2003).  
[45] V. Greco, C. M. Ko, and P. Levai, *Phys. Rev. Lett.* **90**, 202302 (2003).  
[46] V. Greco, C. M. Ko, and P. Levai, *Phys. Rev. C* **68**, 034904 (2003).  
[47] R. J. Fries, B. Muller, C. Nonaka, and S. A. Bass, *Phys. Rev. Lett.* **90**, 202303 (2003).  
[48] R. J. Fries, B. Muller, C. Nonaka, and S. A. Bass, *Phys. Rev. C* **68**, 044902 (2003).  
[49] F.-l. Shao, Q.-b. Xie, and Q. Wang, *Phys. Rev. C* **71**, 044903 (2005).  
[50] H. Georgi, *Lie Algebras In Particle Physics : from Isospin To Unified Theories* (CRC Press, Taylor & Francis, Boca Raton, 2000).  
[51] B. Andersson, G. Gustafson, and B. Soderberg, *Z. Phys. C* **20**, 317 (1983).  
[52] B. Alver *et al.* (PHOBOS), *Phys. Rev. C* **83**, 024913 (2011).  
[53] K. Aamodt *et al.* (ALICE), *Phys. Rev. Lett.* **106**, 032301 (2011).  
[54] B. B. Back *et al.*, *Phys. Rev. Lett.* **91**, 052303 (2003).  
[55] B. B. Back *et al.* (PHOBOS), *Phys. Lett. B* **578**, 297 (2004).  
[56] E. Abbas *et al.* (ALICE), *Phys. Lett. B* **726**, 610 (2013).  
[57] B. Abelev *et al.* (ALICE), *Phys. Lett. B* **720**, 52 (2013).  
[58] G. F. Bertsch and S. Das Gupta, *Phys. Rept.* **160**, 189 (1988).  
[59] J. Cugnon, T. Mizutani, and J. Vandermeulen, *Nucl. Phys. A* **352**, 505 (1981).  
[60] W. Reisdorf *et al.* (FOPI), *Nucl. Phys. A* **848**, 366 (2010).  
[61] J. L. Klay *et al.* (E-0895), *Phys. Rev. C* **68**, 054905 (2003).  
[62] P. Z. Skands, *Phys. Rev. D* **82**, 074018 (2010).  
[63] P. Skands, S. Carrazza, and J. Rojo, *Eur. Phys. J. C* **74**, 3024 (2014).  
[64] B.-H. Sa, D.-M. Zhou, Y.-L. Yan, W.-D. Liu, S.-Y. Hu, X.-M. Li, L. Zheng, G. Chen, and X. Cai, *J. Phys. G* **49**, 065104 (2022).